

Customizing Morphology, Size, and Response Kinetics of Matrix Metalloproteinase-Responsive Nanostructures by Systematic Peptide Design

Jiye Son,^{†,‡,§,||} Daniela Kalafatovic,[†] Mohit Kumar,[†] Barney Yoo,[#] Mike A. Cornejo,[‡] María Contel,^{‡,§,||,⊥} and Rein V. Ulijn^{*,†,§,#,||}

[†]Advanced Science Research Center at The Graduate Center of the City University of New York, 85 Saint Nicholas Terrace, New York, New York 10031, United States

[‡]Department of Chemistry, Brooklyn College, City University of New York, 2900 Bedford Avenue, Brooklyn, New York 11210, United States

Ph.D. Programs in [§]Chemistry, ^{||}Biochemistry, and [⊥]Biology, The Graduate Center of the City University of New York, 365 Fifth Avenue, New York, New York 10016, United States

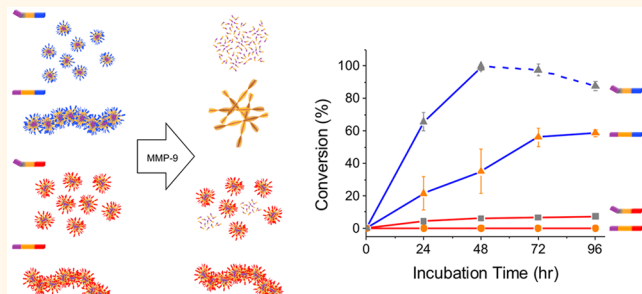
[#]Department of Chemistry, Hunter College, City University of New York, 695 Park Avenue, New York, New York 10065, United States

Supporting Information

ABSTRACT: Overexpression and activation of matrix metalloproteinase-9 (MMP-9) is associated with multiple diseases and can serve as a stimulus to activate nanomaterials for sensing and controlled release. In order to achieve autonomous therapeutics with improved space-time targeting capabilities, several features need to be considered beyond the introduction of an enzyme-cleavable linker into a nanostructure. We introduce guiding principles for a customizable platform using supramolecular peptide nanostructures with three modular components to achieve tunable kinetics and morphology

changes upon MMP-9 exposure. This approach enables (1) fine-tuning of kinetics through introduction of ordered/disordered structures, (2) a 12-fold variation in hydrolysis rates achieved by electrostatic (mis)matching of particle and enzyme charge, and (3) selection of enzymatic reaction products that are either cell-killing nanofibers or disintegrate. These guiding principles, which can be rationalized and involve exchange of just a few amino acids, enable systematic customization of enzyme-responsive peptide nanostructures for general use in performance optimization of enzyme-responsive materials.

KEYWORDS: MMP-responsive, enzyme kinetics, electrostatic enzyme interactions, supramolecular organization, morphology change, self-assembling peptides



Nanomaterials impact biomedicine by taking advantage of their inherent chemical and physical properties to achieve increased circulation lifetime and selective biodistribution *in vivo* and dictate cellular uptake mechanisms,¹ all of which cannot be attained by molecular drugs alone. Another beneficial feature of nanomaterials is the ability to incorporate stimuli-responsive functionalities to enhance selectivity in targeting diseased cells and manipulate drug release profiles.^{2–5} In particular, an inherent biological stimulus such as (over)expression of enzymes can serve as a marker for diseased cells as well as a trigger to facilitate desired changes in

the nanostructure.⁶ Understanding the relationship between properties of nanomaterials, such as size, shape, and charge, with their biodistribution or cellular uptake patterns has allowed researchers to develop refined systems to target specific organs and cells. For example, Discher *et al.* described that the increase in length of flexible filomicelles up to 8 μm increased the circulation lifetime *in vivo* in mice, in comparison

Received: September 27, 2018

Accepted: January 28, 2019

Published: January 28, 2019



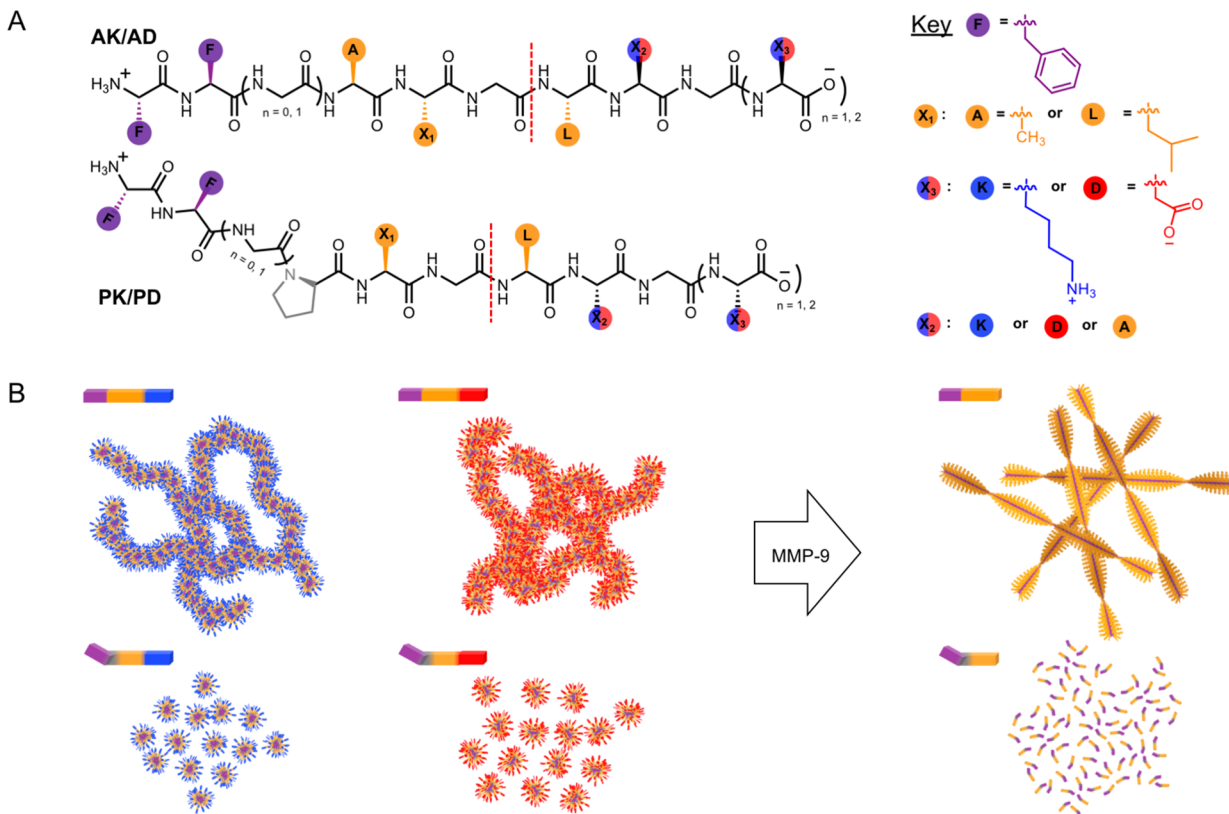


Figure 1. Sequence-dependent peptide nanostructures. (A) Chemical structure and (B) cartoon of self-assembling peptide amphiphiles that respond to MMP-9 action. Positive (blue) or negative (red) charges on the nanoparticle electrostatically recruit or repel MMP-9 to influence enzyme kinetics. Self-assembling (purple) and MMP-9-cleavable segments (gray and/or orange) dictate the susceptibility of the nanostructures to MMP-9 hydrolysis by forming ordered/disordered structures and control the fiber formation or disassembly of the postenzymatic products. Red dashed line indicates the scissile bond.

to shorter filomicelles and spherical vesicles.⁷ Likewise, a thorough investigation is necessary in order to develop design rules for nanomaterials that can engage with the enzymatic stimuli with varying degrees of affinity in order to predetermine response kinetics for the desired enzyme-responsive action (*i.e.*, disassembly, morphology switch, *etc.*).⁶

For instance, an overexpression and activation of matrix metalloproteinase-9 (MMP-9), an enzyme that is crucial to normal behavior of cells such as degradation of extracellular matrix,⁸ is associated with multiple diseases including cancer metastasis,⁹ cardiovascular diseases,¹⁰ arthritis,¹¹ *etc.* Since the introduction of polymeric MMP-responsive materials by Hubbell *et al.*,^{12,13} there have been numerous strategies to exploit this highly disease-relevant enzyme for biomedical applications.^{14–21} One of the challenges in designing MMP-9-responsive nanomaterials is optimizing a cleavable segment that meets the enzyme specificity²² and is concurrently compatible with the nanoparticle system. Another, largely overlooked but important aspect of particle design is regulating the susceptibility of the nanoparticle to the enzyme stimuli through the manipulation of electrostatic properties of nanoparticles to attract or repel enzymes of opposite or same charge²³ and to control the degree of supramolecular organization of the nanoparticle to increase or limit enzyme access to the particle and ultimately influence the observed reaction and response kinetics.²⁴

A further design aspect is the morphology of the particle pre- and postcleavage; there is increasing evidence that enzymatically triggered formation of nanofibers on tumor cells can

cause cytotoxic effects,^{15,25} and Xu *et al.* have extensively studied this mechanism to overcome drug resistance in cancer cells,^{26,27} whereas disintegrating particles may be beneficial for controlled drug release.^{19,20} The anticancer activity of the nanofibers depends on the kinetics of fiber formation, which in turn depends on the interaction between the enzyme and the precursor, as well as the self-assembling ability of the postenzymatic product.²⁸ By employing these strategies, the response behavior of the enzyme-responsive nanomaterials can be optimized to achieve selective and controlled rate of drug release and to introduce additional therapeutic functionalities.

Thus, by using rational design of peptide sequences, we present here a modular platform to customize surface charge, supramolecular organization, and enzyme specificity of peptide nanostructures. We demonstrate the significance of these properties in showing that simple, few amino acid replacements can systematically control enzyme engagement and susceptibility to the enzymatic action which dictates the response kinetics and, in addition, can dictate the action of the nanostructures (degradation or β -sheet formation) to ultimately influence cells' fate.

RESULTS AND DISCUSSION

Rational Design of Peptide Sequences. For this study, we designed self-assembling peptide amphiphiles²⁹ that form stable nanostructures under physiological conditions and undergo morphological change or degradation upon MMP-9 hydrolysis of the peptides, building on our previous work which demonstrated that peptide micelles can encapsulate

Table 1. Single Letter Code of 12 Peptides (Red Dashed Line Indicates Expected Cleavage Site), Critical Aggregation Concentrations of Peptides Determined Using Pyrene ([Figure S9 in Supporting Information](#)), and ζ -Potentials of 5 mM Peptides in 2% PBS (pH 7.4) at 25°C ([Figure S8 in Supporting Information](#))

Position	Peptide Sequence										Charge	CAC ^a	Zeta Potential	
	P ₆	P ₅	P ₄	P ₃	P ₂	P ₁	P' ₁	P' ₂	P' ₃	P' ₄				
	P/A	X ₁	G	L	X ₂	G						pH 7.4	(mM)	Mean (mV) ± Std. dev
1AK	F	F	A	L	G	L	A	G	K	K	+2	0.4	11.5 ± 0.8	
1AD	F	F	A	L	G	L	A	G	D	D	-2	0.6	-34.9 ± 1.1	
1PK	F	F	P	L	G	L	A	G	K	K	+2	0.3	15.4 ± 0.3	
1PD	F	F	P	L	G	L	A	G	D	D	-2	0.5	-38.0 ± 1.7	
2AK	F	F	G	A	L	G	L	K	G	K	+2	0.4	8.2 ± 2.8	
2AD	F	F	G	A	L	G	L	D	G	D	-2	0.6	-30.3 ± 1.4	
2PK	F	F	G	P	L	G	L	K	G	K	+2	0.3	4.1 ± 1.0	
2PD	F	F	G	P	L	G	L	D	G	D	-2	0.7	-41.2 ± 2.3	
3AK	F	F	G	A	A	G	L	K	G	K	+2	0.8	1.3 ± 0.6	
3AD	F	F	G	A	A	G	L	D	G	D	-2	0.5	-7.5 ± 1.8	
3PK	F	F	G	P	A	G	L	K	G	K	+2	0.7	1.1 ± 1.5	
3PD	F	F	G	P	A	G	L	D	G	D	-2	0.5	-28.2 ± 0.7	

^aCritical aggregation concentration.

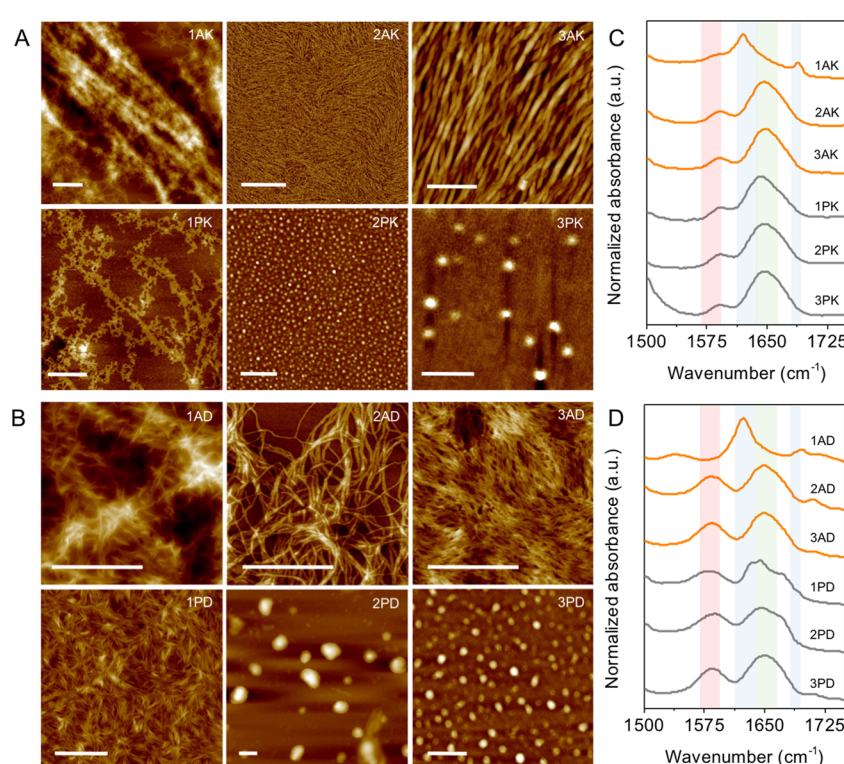


Figure 2. AFM images and FTIR spectra of self-assembled peptide nanostructures. (A,B) 1 AK/AD form large fibers organized in antiparallel β -sheet arrangement; 2–3 AK/AD and 1 PK/PD form elongated worm-like micelles, and 2–3 PK/PD form spherical micelles. Scale bar 500 nm. Additional AFM images can be found in [Figure S5 in Supporting Information](#). (C,D) FTIR spectra of the peptides in amide I region. Red shade highlights the carboxylate groups (1580–1590 cm^{-1}), which can red shift to lower wavenumber (1541 cm^{-1} for 1 AD) upon cation complexation;³⁷ blue shade highlights parallel β -sheet (near 1620 cm^{-1}) and antiparallel β -sheet (additional peak at 1688 cm^{-1}) hydrogen bonding of the peptide backbones, and the green shade highlights disordered hydrogen bonds (1640–1650 cm^{-1}). Peaks are listed in [Table S2 in Supporting Information](#).

doxorubicin and transform into fibrous drug depots upon MMP-9 action.^{21,30} Thus, we created a modular system in which the peptide sequences contain three segments: (1) cationic or anionic hydrophilic segment to modulate enzyme engagement, (2) MMP-9-cleavable segment with ordered or disordered regions to influence enzyme kinetics and predetermine self-assembly or disassembly of postcleavage product, and (3) hydrophobic segment to drive self-assembly

of precursor and of postenzymatic self-assembling product (with potential to bind hydrophobic drugs²¹) ([Figure 1](#)).

To demonstrate the ability to electrostatically recruit MMP-9 (pI = 5.7, net negative charge in physiological pH)³¹ to the peptide particles, we designed a hydrophilic segment in the peptide amphiphiles with cationic or anionic C termini. Each peptide was given a positive (1–3 AK/PK) or negative (1–3 AD/PD) charge using two lysine or two aspartic acid residues,

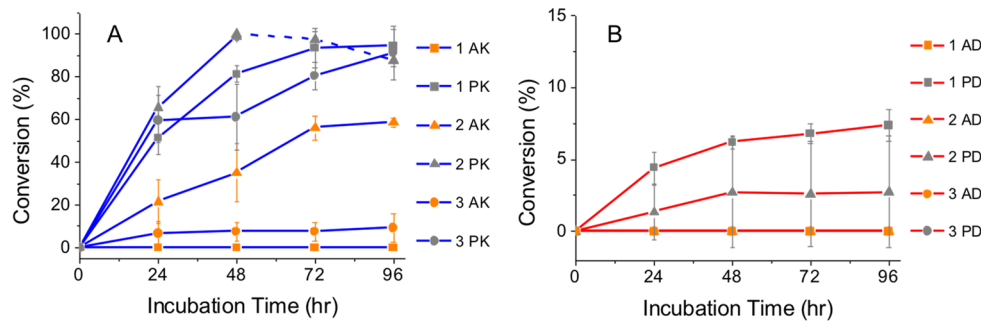


Figure 3. (A) 1–3 AK/PK (1 mM) and (B) 1–3 AD/PD (1 mM) incubated with 100 ng/mL of MMP-9 at 37 °C. Peptides with Pro in P₃ are marked gray and Ala with orange. Average % conversion of peptides to the postenzymatic products (P₁↓P_{1'}) from two separate trials. 1–3 PK showed the highest conversion, and further degradation of the postenzymatic product was observed for 2 PK (blue dash line). Over 50% of 2 AK was cleaved, whereas less than 10% of 3 AK and 1–2 PD was converted, and the rest were not responsive to MMP-9.

thus creating 12 sequences (Table 1). In addition, these surface charges increase solubility of the peptide nanostructures and can be customized to potentially influence cellular uptake and biodistribution.

To achieve MMP-9 specificity and to program the distinct morphologies of the peptide nanostructures and the resulting enzymatic products, we designed the cleavable segment based on data from the MEROPS database,³² which suggests PX₁G↓LX₂G, where ↓ represents the scissile bond and X₁ and X₂ represent positions where there are no significant preferences for a single amino acid. The amino acid positions are designated starting from the scissile bond (red dashed line in Table 1) and are labeled P₁ through P₆ toward the N terminal and P_{1'} and P_{5'} toward the C terminal. Peptides 1–3 PK/PD contain Pro in P₃, which is prevalent in substrates of most MMPs;²² however, Pro is known to disrupt assembly of secondary structures like α -helices and β -sheets in proteins.³³ Therefore, in order to promote fiber formation of the postcleavage enzymatic products, we substituted Pro for Ala in P₃ in 1–3 AK/AD, which is also found in natural substrates of MMP-9.³⁴ In addition, we varied P₂ with small aliphatic residues to observe differences in enzyme specificity and inserted Gly in P₄ to change the self-assembling behavior of peptides and observe the consequent changes in enzyme kinetics.

Finally, to introduce the hydrophobic segment of our amphiphilic peptides, we used the well-known self-assembling sequence of diphenylalanine^{35,36} on the first two positions of the N termini to drive self-assembly of nanostructures prior to enzyme action *via* hydrophobic and aromatic interactions and to form nanofibers in a subset of sequences after enzyme action (1–3 AK/AD). These 12 sequences represent a modular design in which the rate and morphology of the enzymatic response can be customized for desired applications.

Characterization of the Peptide Nanostructures. The 12 peptides were synthesized using Fmoc-based solid-phase peptide synthesis (SPPS), purified on high-performance liquid chromatography (HPLC) using a C₁₈ column, lyophilized in water, and identified by high-resolution mass spectrometry (HRMS) and ¹H nuclear magnetic resonance (NMR) spectroscopy (Figures S1 and S2 in Supporting Information). The critical aggregation concentrations of the peptides were determined using pyrene as a fluorescent probe and ranged between 0.3 and 0.8 mM for cationic peptides and 0.5 and 0.7 mM for anionic peptides (Table 1 and Figure S9 in Supporting Information). The ζ -potentials of the peptide assemblies confirmed the presence of the expected charges (Table 1).

Higher ζ -potentials were observed for the anionic peptides which have negatively charged Asp residues on the free carboxyl termini of the peptides, in comparison to the cationic peptides in which the positive charge of Lys residues is negated by the free C termini (Figure 1A). We note that measurements were made at high concentrations (5 mM) due to the limited light scattering properties of the peptide particles that may have contributed to aggregation, which results in overall lower ζ -potential values (Figure S8 in Supporting Information).

Atomic force microscopy (AFM) images show that AK/AD sequences form one-dimensional nanostructures and PK/PD sequences form spherical nanostructures with the exception of 1 PK/PD (Figure 2A,B). Analysis of Fourier transform infrared (FTIR) spectra reveals that the self-assembly of most of the peptide sequences is not significantly driven by highly ordered hydrogen bonding of the peptide backbones. Instead, the major peaks in the amide I region absorb between 1640 and 1650 cm⁻¹, indicative of disordered hydrogen bonds (shaded green in Figure 2C,D).³⁸ Thus, the major contribution in the formation of these spherical micelles (2–3 PK/PD) or worm-like micelles (1 PK/PD and 2–3 AK/AD) is driven by the formation of a diphenylalanine hydrophobic core solubilized by the hydrophilic lysine or aspartic acid tail.³⁹ In contrast, 1 AK/AD shows prominent characteristics of antiparallel β -sheet arrangement of the peptide backbone which absorbs at 1620 and 1687 cm⁻¹ for 1 AK and at 1623 and 1696 cm⁻¹ for 1 AD (shaded blue in Figure 2C,D). In addition, the carboxylate peak which absorbs at 1580–1590 cm⁻¹ (shaded red in Figure 2C,D) is red-shifted to 1541 cm⁻¹ in 1 AD, indicative of cation complexation, which suggests intermolecular salt bridge formation between the C and N terminal (or aspartic acid residues next to the C terminal), which contributes to the long-range order of the peptide assembly.³⁷ We speculate that these highly ordered nanofibers are caused by the assembly of a linear and rigid backbone of 1 AK/AD in P₆–P₁ (FFALG), and this is clearly evident in 1 PK/PD in which a single amino acid substitution of Ala to Pro in P₃ (FFPLG) creates a kink in the peptide backbone and significantly disrupts the antiparallel β -sheet formation. Furthermore, the addition of Gly in P₄ (FFGAX₁G) in 2–3 AK/AD adds flexibility to the peptide backbone,⁴⁰ which hinders long-range order of the peptide assembly and thus forms smaller nanofibers.

Controlling Enzyme Kinetics. Next, we measured the rate of MMP-9 cleavage of the 12 peptides. Lyophilized peptides were dissolved in phosphate-buffered saline (PBS) supplemented with 1 mM CaCl₂ and 55 μ M ZnCl₂ to be compatible

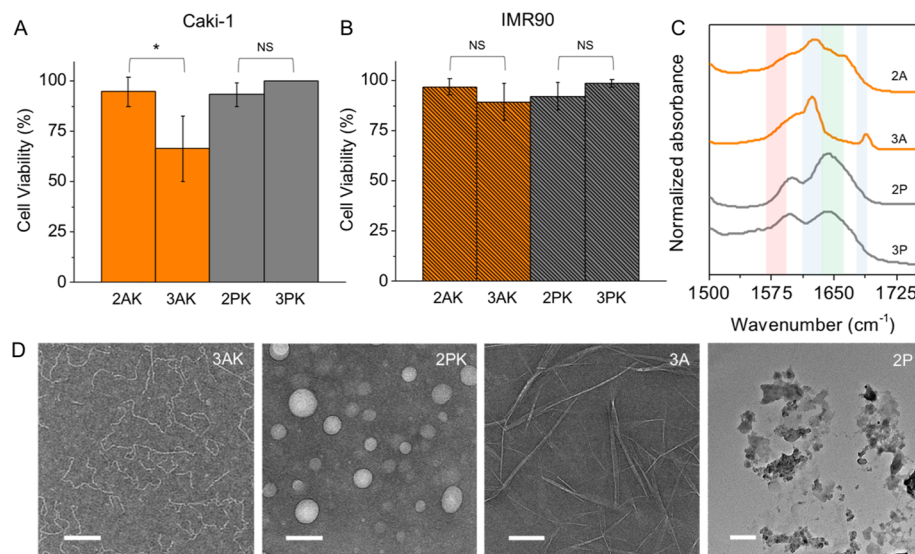


Figure 4. Biocompatibility of peptide nanostructures. Cell viability of human renal cancer cell line, Caki-1, with high expression of MMP-9 (A), and noncancerous human fibroblast, IMR90, with normal expression of the enzyme (B), incubated with 1 mM peptides for 72 h. The peptides are nontoxic to both cell lines, except for 3 AK, which decreased the cell viability of Caki-1 to 66%. (C) FTIR spectra of the postcleavage peptides show that only 3 A forms antiparallel β -sheet peptide fibers, which causes the cytotoxic effects in Caki-1 only. (D) TEM images of 3 AK and 2 PK show formation of worm-like and spherical micelles, respectively, and the postenzymatic products, 3 A and 2 P, which form rigid fibers or random aggregates, respectively. Scale bar 100 nm.

with MMP-9 (a metalloproteinase with zinc- and calcium-dependent catalytic domain), the pH adjusted to 7.4, and sonicated for 10 min to achieve 1 mM of peptide solutions. Next, 100 ng/mL MMP-9 was incubated with peptides at 37 °C, and the reaction was monitored up to 96 h using liquid chromatography–mass spectrometry (LC–MS) to identify and quantify the enzymatic products by calculating the area of the product peak over the initial peptide peak (Figures S3 and S4 in Supporting Information).

Electrostatic Recruitment or Repulsion of MMP-9. Comparing the $P_1 \downarrow P_1'$ enzymatic products, the cationic peptides (Figure 3A) were preferentially cleaved by (anionic) MMP-9. For example, 2 PK had a conversion 12-fold higher than that of 2 PD (Figure 3B). This stark difference resulting from preferential hydrolysis of nanostructures by oppositely charged enzymes has also been observed by Wooley *et al.*²⁴ using polymeric micelles.

Interestingly, the major cleavage site for the cationic peptides was between G↓L in $P_1 \downarrow P_1'$ as anticipated, whereas the major cleavage site for the anionic peptides was between F↓F in $P_6 \downarrow P_5$ with inconsistent results between two separate trials (Table S1 in Supporting Information). It has been reported that MMP-9 cleavage site in peptides of similar length can shift to $P_2 \downarrow P_1$ or $P_1' \downarrow P_2'$,⁴¹ but this drastic shift to $P_6 \downarrow P_5$ suggests that the anionic peptides do not meet MMP-9 specificity. By electrostatic (mis)matching, we are able to recruit or repel MMP-9 to trigger the desired response in the nanomaterial.

Increasing or Limiting Accessibility to Enzymatic Hydrolysis. In addition to the dramatically different conversion rates (and cleavage sites) resulting from electrostatic interactions, we can further fine-tune the rate of enzymatic hydrolysis by achieving enzyme specificity and controlling the degree of order in the supramolecular peptide nanostructures. Of the cationic peptides, sequences with Pro in P_3 (1–3 PK) were almost completely digested by MMP-9 by 96 h. In particular, 1 PK, which forms the smallest micelles of

the three, was completely converted to the enzyme product, FFPLG, in 48 h and continued to be further hydrolyzed between F↓F (dashed blue line in Figure 3A). This demonstrates the biodegradability of peptide nanoparticles, which may be useful for applications where (di)phenylalanine generated amyloid-like toxic fibrils are of concern.⁴² Overall, 1–3 PK were cleaved to completion at a similar rate due to the preferred Pro residue in P_3 , and the subtle differences in the peptide sequences did not affect the enzymatic hydrolysis rates.

In the case of 1–3 AK, significant differences were observed due to the degree of supramolecular organization of the nanostructures. 3 AK, which has the highest critical aggregation concentration (CAC) value of 0.8 mM, had a low conversion (below 10% by 96 h), whereas 2 AK with a lower CAC value of 0.4 mM had the highest conversion (up to 60% by 96 h), and no cleavage was observed for 1 AK (CAC value 0.4 mM). These data suggest that the kinetics of the enzyme hydrolysis are determined by the supramolecular order of the peptide assemblies rather than the hydrolysis of unassembled peptide monomers. The slight difference of introducing a glycine residue in the sequences of 2 AK and 1 AK (between diphenylalanine and alanine) contributes to a major change in the morphology of the two nanostructures. 2 AK, which has a more flexible peptide backbone due to the insertion of Gly residue in P_4 , forms disordered hydrogen bonds (Figure 2C) that leads to the formation of smaller fibrils (Figure 2A and Figure SSA in Supporting Information) and is susceptible to MMP-9 hydrolysis. However, without the Gly residue, the rigid peptide backbone of 1 AK in P_6 – P_1 arranges in an antiparallel β -sheet configuration (Figure 2C) and forms fibers that are microns long (Figure 2A and Figure SSA in Supporting Information). These highly organized fibers are less susceptible to enzyme degradation, especially for the endopeptidase MMP-9, which has been observed to bind to type I fibril collagen, a large extracellular matrix component, but cannot digest it until it is in the denatured gelatin form.⁴³ From this set of 12 peptides, it is clear that we can dramatically

control the rate and specificity of MMP-9 hydrolysis through systematic exchange of amino acids.

Biocompatibility of Peptide Nanostructures *in Vitro*.

Moving forward, we chose to test the biocompatibility of the two peptides that were active against MMP-9, 2 AK and 3 AK, and their Pro analogous peptides, 2 PK and 3 PK. We chose a human clear cell renal cell carcinoma line, Caki-1, because tissues from patients with this type of kidney cancer show significantly higher expression of MMP-9 mRNA, with increasingly higher expression in advanced tumor stages.⁴⁴ As a control, we chose a noncancerous human lung fibroblast cell line, IMR90, which was reported to have negligible expression of MMP-9 mRNA.⁴⁵ One millimolar of the peptides was incubated with Caki-1 and IMR90 cells at 37 °C for 72 h, and the cell viability was determined using the Presto Blue assay (Figure 4A,B). The peptides are nontoxic to both cell lines with cell viabilities over 90%, except for 3 AK, which forms β -sheet fiber postcleavage and decreased the cell viability of Caki-1 cells to 66%, despite the observed low conversion (Figure 3A).

Nanofibers Induce Selective Toxicity in Cancer Cells.

In order to understand the effects of the postcleavage products *in vitro*, we synthesized the hydrophobic N terminal fragments of the resulting enzymatic products (herein referred to as 2–3 A/P) by SPPS and studied their self-assembly behaviors using FTIR, AFM, and TEM. The full characterization of 1–3 A/P can be found in Supporting Information (HRMS, ¹H NMR, AFM, FTIR, and additional TEM). Distinct differences can be observed by peptides with Ala in P₃ (2–3 A), which formed ordered structures, and peptides with Pro in P₃ (2–3 P), which was expected not to self-assemble due to the Pro disrupting formation of ordered hydrogen bonds. FTIR spectra of the nonassembling peptides (Figure 4C, gray lines) show absorptions at 1643 and 1653 cm⁻¹ for 2 P and 3 P, respectively, which is observed for amides of peptide backbones with disordered hydrogen bonds. A mixture of parallel β -sheet (1628 cm⁻¹) and disordered (1643 cm⁻¹) hydrogen bonds was observed for 2 A. In contrast, 3 A absorbs at 1624 and 1688 cm⁻¹, which are distinct characteristic peaks of antiparallel β -sheet hydrogen bonds (Figure 4C, orange lines). TEM images (Figure 4D) show that the precursor 2 PK forms spherical particles which, when converted to 2 P, disassemble and remain as random aggregates. In comparison, precursor 3 AK forms flexible fibers, and the postenzymatic product 3 A forms ordered rigid β -sheet fibers. Enzyme-triggered fibers which form on or near the cell surface of cancer cells that produce the enzyme stimuli are known to be cytotoxic to the cells.⁴⁶ Likewise, the observed decrease in viability of Caki-1 cells treated with 3 AK is most likely due to the formation of toxic antiparallel β -sheet nanofibers (3 A) that are selectively triggered to form by the overexpressed MMP-9 in the diseased cells.¹⁶ This effect is not observed in the control cell line, IMR90, where overexpression of MMP-9 is not expected.

CONCLUSION

In conclusion, we have created a modular system of self-assembling peptide nanostructures to customize surface charge and supramolecular order to control enzyme kinetics and response action. These peptide nanostructures are nontoxic and biodegradable, and after enzyme action, the nonassembling products remain nontoxic while the β -sheet nanofiber forming products can selectively kill cancer cells. The kinetics

of nanoparticles is important in biomedical applications in which the rate of enzyme responsiveness should be regulated (*i.e.*, predetermined drug release profile, degradation rate of hydrogels, *etc.*). In addition, the morphology of the nanoparticles should be logically designed to achieve optimal function of the precursors (*i.e.*, manipulation of cellular uptake, biodistribution, *etc.*) and of the postenzymatic product (*i.e.*, biodegradability or therapeutic nanofiber/drug depots, *etc.*).

METHODS

Solid-Phase Peptide Synthesis. Fluorenylmethyloxycarbonyl (Fmoc)-protected amino acids and preloaded Wang resins were purchased from Bachem. Peptides were synthesized on CEM Liberty Blue microwave-assisted solid-phase peptide synthesizer using ~1:5 resin to amino acid ratio and excess diisopropylcarbodiimide, Oxyma (ethyl(hydroxymino)cyanooacetate), and 20% piperidine in dimethylformamide. The complete peptide-loaded resins were washed three times in dichloromethane, followed by three washes in diethyl ether on a filtration column. The peptides were cleaved from the resins, and side chain protecting groups were removed by reacting with a TFA cocktail (95% trifluoroacetic acid, 2.5% triisopropyl silane, and 2.5% water) for 2 h. The cleaved peptides were recovered by removing the TFA cocktail, followed by precipitation in cold diethyl ether. Peptides were washed three times in cold diethyl ether, using a centrifuge to decant the supernatant. The crude peptides were dissolved in Milli-Q water and lyophilized.

Preparatory High-Performance Liquid Chromatography. Lyophilized crude peptides were dissolved in 50% acetonitrile in water containing 0.1% TFA and purified through a preparatory C₁₈ column on the Thermo Scientific Dionex Ultimate 3000. Acetonitrile was removed from the collected fragments on a rotary evaporator before lyophilization. Purified peptides were dissolved in 10 mM HCl solution to make 1 mM peptide solution and lyophilized to remove residual TFA salts.

High-Resolution Mass Spectrometry. HRMS data were obtained on an Agilent 6550 QToF, with a dual sprayer ESI source, coupled to an Agilent 1290 Infinity LC system. Samples were analyzed by flow injection analysis using a mobile phase of 50% acetonitrile in water (0.1% formic acid) with a flow rate of 0.4 mL/min.

¹H Nuclear Magnetic Resonance Spectroscopy. NMR spectra were recorded in a Bruker AV400 at 400 MHz. Chemical shifts (δ) are given in parts per million using D₂O as solvent.

Assay To Determine the Rate of MMP-9 Cleavage of Peptide Sequences. MMP-9 (catalytic domain) (human), (recombinant, *Escherichia coli*) was purchased from Enzo. The purchased enzyme solution was defrosted and aliquots were made for storage in -80 °C. The 1 mM peptides were prepared in PBS (2.7 mM KCl, 137 mM NaCl, supplemented with 1 mM CaCl₂, 55 μ M ZnCl₂, pH 7.4), and the pH was adjusted to 7.4 using 0.5 M NaOH or 0.5 M HCl. Peptides were sonicated for 10 min to facilitate self-assembly and then incubated at 37 °C in a stationary heat block. Peptide samples for $t = 0$ analysis were reserved, and 100 ng/mL of MMP-9 (stock aliquot was diluted to 10,000 ng/mL in PBS) was gently mixed into the 1 mM peptide solution. Reaction samples were taken every 24 h for LC-MS analysis.

Liquid Chromatography-Mass Spectrometry. Thirty microliters of the MMP-9 reaction solution (or peptide only solution at $t = 0$) was directly added to 50% acetonitrile in water containing 0.1% TFA. Samples were analyzed on an LC-MS system comprising an Agilent 1200 LC system coupled to an Agilent 6340 ion trap mass spectrometer. Samples were injected onto an Agilent Zorbax column (SB-C8, 5 μ M, 2.1 × 50 mm) using a gradient of 2–50% acetonitrile in water (0.1% formic acid) at a flow rate of 200 μ L/min over 10 min followed by a 2 min wash step with 95% acetonitrile.

Atomic Force Microscopy. AFM images were taken on Bruker Dimension FastScan using FASTSCAN-B tip on fast scan mode. Peptide solution (1 mM) was prepared in phosphate buffer (pH 7.4),

sonicated for 10 min, and drop casted on freshly cleaved mica and allowed to dry for 48 h before imaging.

Transmission Electron Microscopy. TEM images were taken on FEI Titan Halo 80-300 microscope. Peptide solution (1 mM) was prepared in 10 mM phosphate buffer (pH 7.4) sonicated for 10 min, and 5 μ L of the solution was drop casted on a carbon film grid (400 mesh, copper) and dried completely. To the dry grid was added 5 μ L of Milli-Q water and quickly blotted to wash away the phosphate salts and dried completely. Finally, 5 μ L of methylamine vanadate-based negative stain (NanoVan by Nanoprobe) was drop casted, blotted away, and dried completely.

Fourier Transform Infrared Spectroscopy. Absorbance spectra were taken from 4000 to 800 cm^{-1} with 64 scans at 4 cm^{-1} resolution on the Bruker Vertex 70 spectrometer. Peptide solution (20 mM) was prepared in deuterated phosphate buffer (pH 8); pH was adjusted to 7.4 using 0.5 M NaOH or 0.5 M HCl and sonicated for 10 min. Five microliters of sample solution was drop casted between two CaF_2 cells with PTFE spacers (12 μm thickness \times 13 mm diameter). For analysis, deuterated phosphate buffer absorbance spectra were subtracted from the sample absorbance and normalized from 1560 to 1655 cm^{-1} .

ζ -Potential. The ζ -potential measurements were made on Anton Paar Litesizer 500 Particle Analyzer. Peptide samples (5 mM) were prepared in 2% PBS, and the pH was adjusted to 7.4 using dilute NaOH and HCl. Fifty microliters of sample was pipetted into Univette low volume cuvette, and three series of measurements were made at 25 °C using Smoluchowski approximation.

Critical Aggregation Concentration. Peptides (1 mM) were prepared in PBS, and the pH was adjusted to 7.4 using 0.5 M NaOH or 0.5 M HCl and serially diluted in PBS with thorough vortexing. Peptide solutions were incubated in 50 °C for 15 min, then 2 μ L of stock pyrene solution (100 μM in methanol) was added to 100 μL of each peptide solution, gently mixed, and incubated for 5 min at 50 °C, then finally cooled to room temperature to coassemble the peptides with pyrene molecules. Pyrene emission spectra was measured from 350 to 450 nm ($\lambda_{\text{ex}} = 310$ nm) in a microfluorescence cuvette (3 mm path length) on a Jasco FP-8500 spectrophotometer (measurement parameter: 20 nm excitation and 1 nm emission bandwidth, 0.2 s response, medium sensitivity, 0.2 nm data interval, at 200 nm/min). The CAC was determined by plotting the ratio between intensities of the third to first peak of the pyrene emission spectra. Increasing peptide concentrations were measured in 0.1 mM increments until the slope of the plot had changed, and simultaneously the third peak shifted from 382.4 to 384.4 nm and the first peak shifted from 371.8 to 373.4 nm.

Cell Lines. Human clear cell renal cell carcinoma line Caki-1 was newly obtained for these studies from the American Type Culture Collection (ATCC) (Manassas, Virginia, USA) and cultured in Roswell Park Memorial Institute (RPMI-1640) (Mediatech Inc., Manassas, VA) media containing 10% fetal bovine serum, certified, heat-inactivated, U.S. origin (FBS) (Gibco, Life Technologies, USA), 1% minimum essential media nonessential amino acids (NEAA, Mediatech) and 1% penicillin–streptomycin (PenStrep, Mediatech). IMR90 (human fetal lung fibroblast) cells were purchased from ATCC (Manassas, Virginia, USA) and maintained in Dulbecco's modified Eagle's medium (Mediatech) supplemented with 10% FBS, 1% NEAA, and 1% PenStrep.

Cell Viability Assay. Human fetal lung fibroblast (IMR90) and human clear cell renal cell carcinoma cells (Caki-1) were seeded in a 96-well flat bottom microplate (BioLite Microwell Plate, Fisher Scientific, Waltham, MA). For IMR90, we used 6.0×10^3 cells per well, and for Caki-1, we used 5.6×10^3 cells per well in 90 μL of complete phenol red free cell culture media. The cells were allowed to grow for 24 h at 37 °C and 5% CO₂ in a humidified incubator. Peptide solutions (10 mM) were prepared in phosphate buffer saline, pH adjusted to 7.4 using NaOH or HCl, and sonicated for 10 min. Then 10 μL of each sample was added into wells containing 90 μL of media (in triplicate). Following the administration of the peptides, cells were incubated for 72 h at 37 °C under 5% CO₂. After each period of incubation, Presto Blue (Life Technologies, Carlsbad, CA)

was used as an indicator of cellular toxicity; 11 μL of Presto Blue was added to each well and incubated for 1 h at 37 °C under 5% CO₂. The 96-well plate was then analyzed using a multimode plate-reader BioTek Microplate Reader (BioTek U.S., Winooski, VT) at 530 and 590 nm wavelength. The percentage of surviving cells was calculated as a normalized ratio of the fluorescence intensity between cells treated with media and phosphate buffer saline alone.

ASSOCIATED CONTENT

Supporting Information

The Supporting Information is available free of charge on the ACS Publications website at DOI: [10.1021/acsnano.8b07401](https://doi.org/10.1021/acsnano.8b07401).

MMP-9 cleavage studies by LC–MS and characterization of peptides using HRMS, ¹H NMR, AFM, TEM, FTIR, ζ -potential, and CAC studies ([PDF](#))

AUTHOR INFORMATION

Corresponding Author

*E-mail: rein.ulijn@asrc.cuny.edu.

ORCID

Jiye Son: [0000-0003-3482-9813](https://orcid.org/0000-0003-3482-9813)

María Contel: [0000-0002-9825-4441](https://orcid.org/0000-0002-9825-4441)

Rein V. Uljin: [0000-0002-7138-1213](https://orcid.org/0000-0002-7138-1213)

Notes

The authors declare no competing financial interest.

ACKNOWLEDGMENTS

LC–MS analysis was performed at Hunter Mass Spectrometry, supported by the City University of New York. We thank the Tow Foundation Graduate Fellowship from the MSKCC Center for Molecular Imaging and Nanotechnology (J.S.), the SEED Grant CUNY-Advanced Science Research Center Program (M.C.), and the National Cancer Institute (NCI) and the National Institute for General Medical Sciences (NIGMS) Grants 1SC1CA182844 and 2SC1 GM127278-05A1 (M.C.).

REFERENCES

- (1) Kinnear, C.; Moore, T. L.; Rodriguez-Lorenzo, L.; Rothen-Rutishauser, B.; Petri-Fink, A. Form Follows Function: Nanoparticle Shape and Its Implications for Nanomedicine. *Chem. Rev.* **2017**, *117*, 11476–11521.
- (2) Blum, A. P.; Kammerer, J. K.; Rush, A. M.; Callmann, C. E.; Hahn, M. E.; Gianneschi, N. C. Stimuli-Responsive Nanomaterials for Biomedical Applications. *J. Am. Chem. Soc.* **2015**, *137*, 2140–2154.
- (3) Mura, S.; Nicolas, J.; Couvreur, P. Stimuli-Responsive Nanocarriers for Drug Delivery. *Nat. Mater.* **2013**, *12*, 991–1003.
- (4) Chen, G.; Roy, I.; Yang, C.; Prasad, P. N. Nanochemistry and Nanomedicine for Nanoparticle-Based Diagnostics and Therapy. *Chem. Rev.* **2016**, *116*, 2826–2885.
- (5) Soukasene, S.; Toft, D. J.; Moyer, T. J.; Lu, H.; Lee, H.-K.; Standley, S. M.; Cryns, V. L.; Stupp, S. I. Antitumor Activity of Peptide Amphiphile Nanofiber-Encapsulated Camptothecin. *ACS Nano* **2011**, *5*, 9113–9121.
- (6) Zelzer, M.; Todd, S. J.; Hirst, A. R.; McDonald, T. O.; Uljin, R. V. Enzyme Responsive Materials: Design Strategies and Future Developments. *Biomater. Sci.* **2013**, *1*, 11–39.
- (7) Christian, D. A.; Cai, S.; Garбуzaenko, O. B.; Harada, T.; Zajac, A. L.; Minko, T.; Discher, D. E. Flexible Filaments for *In Vivo* Imaging and Delivery. *Mol. Pharmaceutics* **2009**, *6*, 1343–1352.
- (8) Visse, R.; Nagase, H. Matrix Metalloproteinases and Tissue Inhibitors of Metalloproteinases: Structure, Function, and Biochemistry. *Circ. Res.* **2003**, *92*, 827–839.

- (9) Overall, C. M.; Kleifeld, O. Tumour Microenvironment – Opinion: Validating Matrix Metalloproteinases as Drug Targets and Anti-Targets for Cancer Therapy. *Nat. Rev. Cancer* **2006**, *6*, 227–239.
- (10) Kai, H.; Ikeda, H.; Yasukawa, H.; Kai, M.; Seki, Y.; Kuwahara, F.; Ueno, T.; Sugi, K.; Imaizumi, T. Peripheral Blood Levels of Matrix Metalloproteinases-2 and -9 Are Elevated in Patients with Acute Coronary Syndromes. *J. Am. Coll. Cardiol.* **1998**, *32*, 368–372.
- (11) Burrage, P. S.; Mix, K. S.; Brinckerhoff, C. E. Matrix Metalloproteinases: Role in Arthritis. *Front. Biosci., Landmark Ed.* **2006**, *11*, 529–543.
- (12) West, J. L.; Hubbell, J. A. Polymeric Biomaterials with Degradation Sites for Proteases Involved in Cell Migration. *Macromolecules* **1999**, *32*, 241–244.
- (13) Lutolf, M. P.; Hubbell, J. A. Synthetic Biomaterials as Instructive Extracellular Microenvironments for Morphogenesis in Tissue Engineering. *Nat. Biotechnol.* **2005**, *23*, 47–55.
- (14) Patterson, J.; Hubbell, J. A. Enhanced Proteolytic Degradation of Molecularly Engineered PEG Hydrogels in Response to MMP-1 and MMP-2. *Biomaterials* **2010**, *31*, 7836–7845.
- (15) Tanaka, A.; Fukuoka, Y.; Morimoto, Y.; Honjo, T.; Koda, D.; Goto, M.; Maruyama, T. Cancer Cell Death Induced by the Intracellular Self-Assembly of an Enzyme-Responsive Supramolecular Gelator. *J. Am. Chem. Soc.* **2015**, *137*, 770–775.
- (16) Zhou, J.; Du, X.; Yamagata, N.; Xu, B. Enzyme-Instructed Self-Assembly of Small D-Peptides as a Multiple-Step Process for Selectively Killing Cancer Cells. *J. Am. Chem. Soc.* **2016**, *138*, 3813–3823.
- (17) Callmann, C. E.; Barback, C. V.; Thompson, M. P.; Hall, D. J.; Mattrey, R. F.; Gianneschi, N. C. Therapeutic Enzyme-Responsive Nanoparticles for Targeted Delivery and Accumulation in Tumors. *Adv. Mater.* **2015**, *27*, 4611–4615.
- (18) Lin, Y.-A.; Ou, Y.-C.; Cheetham, A. G.; Cui, H. Rational Design of MMP Degradable Peptide-Based Supramolecular Filaments. *Biomacromolecules* **2014**, *15*, 1419–1427.
- (19) Kulkarni, P. S.; Haldar, M. K.; Nahire, R. R.; Katti, P.; Ambre, A. H.; Muñonen, W. W.; Shabb, J. B.; Padi, S. K. R.; Singh, R. K.; Borowicz, P. P.; Srivastava, D. K.; Katti, K. S.; Reindl, K.; Guo, B.; Mallik, S. MMP-9 Responsive PEG Cleavable Nanovesicles for Efficient Delivery of Chemotherapeutics to Pancreatic Cancer. *Mol. Pharmaceutics* **2014**, *11*, 2390–2399.
- (20) Kim, K.; Bae, B.; Kang, Y. J.; Nam, J.-M.; Kang, S.; Ryu, J.-H. Natural Polypeptide-Based Supramolecular Nanogels for Stable Noncovalent Encapsulation. *Biomacromolecules* **2013**, *14*, 3515–3522.
- (21) Kalafatovic, D.; Nobis, M.; Son, J.; Anderson, K. I.; Ulijn, R. V. MMP-9 Triggered Self-Assembly of Doxorubicin Nanofiber Depots Halts Tumor Growth. *Biomaterials* **2016**, *98*, 192–202.
- (22) Eckhard, U.; Huesgen, P. F.; Schilling, O.; Bellac, C. L.; Butler, G. S.; Cox, J. H.; Dufour, A.; Goebeler, V.; Kappelhoff, R.; Keller, U.; Klein, T.; Lange, P. F.; Marino, G.; Morrison, C. J.; Prudova, A.; Rodriguez, D.; Starr, A. E.; Wang, Y.; Overall, C. M. Active Site Specificity Profiling of the Matrix Metalloproteinase Family: Proteomic Identification of 4300 Cleavage Sites by Nine MMPs Explored with Structural and Synthetic Peptide Cleavage Analyses. *Matrix Biol.* **2016**, *49*, 37–60.
- (23) Thornton, P. D.; Mart, R. J.; Webb, S. J.; Ulijn, R. V. Enzyme-Responsive Hydrogel Particles for the Controlled Release of Proteins: Designing Peptide Actuators to Match Payload. *Soft Matter* **2008**, *4*, 821–827.
- (24) Samarajeewa, S.; Zentay, R. P.; Jhurry, N. D.; Li, A.; Seetho, K.; Zou, J.; Wooley, K. L. Programmed Hydrolysis of Nanoassemblies by Electrostatic Interaction-Mediated Enzymatic-Degradation. *Chem. Commun.* **2014**, *50*, 968–970.
- (25) Pires, R. A.; Abul-Haija, Y. M.; Costa, D. S.; Novoa-Carballal, R.; Reis, R. L.; Ulijn, R. V.; Pashkuleva, I. Controlling Cancer Cell Fate Using Localized Biocatalytic Self-Assembly of an Aromatic Carbohydrate Amphiphile. *J. Am. Chem. Soc.* **2015**, *137*, 576–579.
- (26) Wang, H.; Feng, Z.; Wang, Y.; Zhou, R.; Yang, Z.; Xu, B. Integrating Enzymatic Self-Assembly and Mitochondria Targeting for Selectively Killing Cancer Cells without Acquired Drug Resistance. *J. Am. Chem. Soc.* **2016**, *138*, 16046–16055.
- (27) Feng, Z.; Wang, H.; Wang, S.; Zhang, Q.; Zhang, X.; Rodal, A. A.; Xu, B. Enzymatic Assemblies Disrupt the Membrane and Target Endoplasmic Reticulum for Selective Cancer Cell Death. *J. Am. Chem. Soc.* **2018**, *140*, 9566–9573.
- (28) Feng, Z.; Wang, H.; Chen, X.; Xu, B. Self-Assembling Ability Determines the Activity of Enzyme-Instructed Self-Assembly for Inhibiting Cancer Cells. *J. Am. Chem. Soc.* **2017**, *139*, 15377–15384.
- (29) Zhang, S. Fabrication of Novel Biomaterials through Molecular Self-Assembly. *Nat. Biotechnol.* **2003**, *21*, 1171–1178.
- (30) Kalafatovic, D.; Nobis, M.; Javid, N.; Frederix, P. W. J. M.; Anderson, K. I.; Saunders, B. R.; Ulijn, R. V. MMP-9 Triggered Micelle-to-Fibre Transitions for Slow Release of Doxorubicin. *Biomater. Sci.* **2015**, *3*, 246–249.
- (31) Jaiswal, A.; Chhabra, A.; Malhotra, U.; Kohli, S.; Vibha Rani, V. Comparative Analysis of Human Matrix Metalloproteinases: Emerging Therapeutic Targets in Diseases. *Bioinformation* **2011**, *6*, 23–30.
- (32) Rawlings, N. D.; Barrett, A. J.; Finn, R. Twenty Years of the MEROPS Database of Proteolytic Enzymes, Their Substrates and Inhibitors. *Nucleic Acids Res.* **2016**, *44*, 343–350.
- (33) Woolfson, D. N.; Williams, D. H. The Influence of Proline Residues on α -Helical Structure. *FEBS Lett.* **1990**, *277*, 185–188.
- (34) Kridel, S. J.; Chen, E.; Kotra, L. P.; Howard, E. W.; Mobashery, S.; Smith, J. W. Substrate Hydrolysis by Matrix Metalloproteinase-9. *J. Biol. Chem.* **2001**, *276*, 20572–20578.
- (35) Reches, M.; Gazit, E. Casting Metal Nanowires Within Discrete Self-Assembled Peptide Nanotubes. *Science* **2003**, *300*, 625–627.
- (36) Gazit, E. Self-Assembled Peptide Nanostructures: The Design of Molecular Building Blocks and Their Technological Utilization. *Chem. Soc. Rev.* **2007**, *36*, 1263–1269.
- (37) Barth, A. The Infrared Absorption of Amino Acid Side Chains. *Prog. Biophys. Mol. Biol.* **2000**, *74*, 141–173.
- (38) Fleming, S.; Ulijn, R. V. Design of Nanostructures Based on Aromatic Peptide Amphiphiles. *Chem. Soc. Rev.* **2014**, *43*, 8150–8177.
- (39) Shimada, T.; Lee, S.; Bates, F. S.; Hotta, A.; Tirrell, M. Wormlike Micelle Formation in Peptide-Lipid Conjugates Driven by Secondary Structure Transformation of the Headgroups. *J. Phys. Chem. B* **2009**, *113*, 13711–13714.
- (40) Pace, C. N.; Scholtz, J. M. A Helix Propensity Scale Based on Experimental Studies of Peptides and Proteins. *Biophys. J.* **1998**, *75*, 422–427.
- (41) Huang, Y.; Shi, J.; Yuan, D.; Zhou, N.; Xu, B. Length-Dependent Proteolytic Cleavage of Short Oligopeptides Catalyzed by Matrix Metalloproteinase-9: Proteolytic Cleavage of Short Oligopeptides by MMPs. *Biopolymers* **2013**, *100*, 790–795.
- (42) Adler-Abramovich, L.; Vaks, L.; Carny, O.; Trudler, D.; Magno, A.; Caflisch, A.; Frenkel, D.; Gazit, E. Phenylalanine Assembly into Toxic Fibrils Suggests Amyloid Etiology in Phenylketonuria. *Nat. Chem. Biol.* **2012**, *8*, 701–706.
- (43) Collier, I. E.; Legant, W.; Marmer, B.; Lubman, O.; Saffarian, S.; Wakatsuki, T.; Elson, E.; Goldberg, G. I. Diffusion of MMPs on the Surface of Collagen Fibrils: The Mobile Cell Surface – Collagen Substratum Interface. *PLoS One* **2011**, *6*, e24029.
- (44) Qiao, Z.; Li, Y.; Lu, H.; Wang, K.; Xu, W. Expression of Tissue Levels of Matrix Metalloproteinases and Tissue Inhibitors of Metalloproteinases in Renal Cell Carcinoma. *World J. Surg. Oncol.* **2013**, *11*, 1.
- (45) Giambardini, T. A.; Grant, G. M.; Taylor, G. P.; Hay, R. J.; Maher, V. M.; McCormick, J. J.; Klebe, R. J. Overview of Matrix Metalloproteinase Expression in Cultured Human Cells. *Matrix Biol.* **1998**, *16*, 483–496.
- (46) Zhou, J.; Xu, B. Enzyme-Instructed Self-Assembly: A Multistep Process for Potential Cancer Therapy. *Bioconjugate Chem.* **2015**, *26*, 987–999.